

Polarization of pulsar radiation in the two-pole caustic model and in the outer gap model*

J. Dyks^{1,2}, A. K. Harding¹, and B. Rudak²

November 5, 2018

Abstract

We present linear polarization characteristics of pulsar radiation as predicted by two models of high-energy radiation from extended regions in the outer magnetosphere: the recently proposed two-pole caustic (TPC) model (Dyks & Rudak 2003), and the outer gap (OG) model (Romani & Yadigaroglu 1995 – RY95; Cheng, Ruderman & Zhang 2000).

1 Two-pole caustic model vs outer gap model

The two-pole caustic model differs from the outer gap model in that its emission region extends below the null charge surface toward the polar cap (Fig. 1). The TPC model discards emission from regions close to the light cylinder (ie. from $\rho \gtrsim 0.8R_{lc}$ where ρ is the distance from the rotation axis and R_{lc} is the radius of the light cylinder), because the dynamics of electrons and the geometry of the magnetic field is not known there whereas the OG model includes this emission near the light cylinder. The TPC model assumes that the bulk of photon emission occurs on the last open field lines ($r_{ovc} = 1$) whereas the OG model employs $r_{ovc} = 0.8 - 0.9$, where r_{ovc} is the “open volume coordinate” corresponding to the location of the gamma-ray emitting magnetic field lines at the star surface ($r_{ovc} = 1$ – rim of the polar cap; $r_{ovc} \sim 0$ – central parts of the polar cap). Due to these differences in geometry of the emission region, the TPC model uses the double-pole interpretation of the widely separated double peaks of some gamma-ray pulsars (Crab, Vela, Geminga, B1951+32, B1046–58). The OG model offers the single-pole interpretation. Strong differences between the emission patterns of the two models, and between predicted lightcurves are shown in Fig. 2.

¹NASA Goddard Space Flight Center, Greenbelt, MD, USA

²Nicolaus Copernicus Astronomical Center, Toruń, Poland

*Poster presented at the X-Ray Polarimetry Workshop, SLAC, Stanford, California, 9 – 11 February 2004.

2 Calculation method

The vacuum dipole with the sweepback effect is used. Uniform intensity per unit length of the magnetic field lines is assumed in the corotating frame (CF). The electric field vector of the received radiation \vec{E}_w is taken along the local acceleration vector \vec{a} at the emission point (RY95 took $\vec{E}_w \parallel \vec{\rho}_{\text{curv}}$ where $\vec{\rho}_{\text{curv}}$ is the local curvature radius of the magnetic field lines in the CF). The intrinsic polarization degree of 80% was assumed. To account for possible overlap of emissions from different regions of the magnetosphere, appropriate handling of Stokes parameters I , Q , U was performed. The parameters were finally transformed to the position angle ψ and the polarization degree $P[\%]$.

3 Polarization data

So far, “high-energy” data on pulsar polarization are limited to the optical data on the Crab pulsar (Jones et al. 1981; Smith et al. 1988; Graham-Smith et al. 1996; Romani et al. 2001; Kanbach et al. 2003) and optical data on B0656+14 (Kern et al. 2003). The left column of Fig. 3 presents the lightcurve (top panel), the position angle (PA) curve (middle panel), and the degree of polarization (bottom panel) for the Crab pulsar observed with the OPTIMA instrument (Kanbach et al. 2003; poster at this workshop). Two fast swings of position angle and very low polarization degree at both peaks are noticeable. Beyond the peaks the signal is apparently dominated by a component with fixed position angle, so far of unrecognized origin. The right column shows the data with the constant component subtracted (Kellner 2002). A similar anticorrelation between the total flux and the polarization degree has also been observed in the optical for B0656+14 (Kern et al. 2003).

4 Modelled polarization properties of pulsars

Radiation characteristics calculated for the TPC model with the dipole inclination $\alpha = 70^\circ$ are presented in Fig. 4, which consists of nine three-panel frames for nine different viewing angles ζ_{obs} measured from the rotation axis (their values are displayed in the upper right corner of each frame). Each frame shows the lightcurve (top), the position angle ψ (middle), and the polarization degree (bottom). Photon emission assumed in this calculation was dominated by, but not limited to, the last open field lines. Emission from neighboring magnetic field lines (with different r_{ovc}) was weighted by $\exp[0.5(r_{\text{ovc}} - 1)^2/\sigma^2]$ with $\sigma = 0.025$, ie. a Gaussian profile centered at the polar cap rim was assumed.

For most viewing angles the double-peaked lightcurves can be discerned. Associated with the peaks are fast changes of ψ and minima in $P[\%]$ which are similar to those observed in the Crab. The fast change of ψ at the leading peak near $\phi \simeq 0.1$ is due to caustic effects and is faster on the trailing side of the peak, than on the leading side, in agreement with the Crab data. This swing is a very stable feature whereas the swing at the trailing peak is very sensitive to model parameters. The minima in $P[\%]$ have the form of “double dips” – the leading dip in each pair is due to a combination of caustic effects and overlapping emission from the neighboring magnetic field lines with slightly different r_{ovc} . The dips which lag the maxima in intensity

arise because of superposition of radiation patterns from opposite magnetic hemispheres. For more details see Dyks, Harding & Rudak 2004.

In Fig. 5 results for the OG model are shown with the same layout as before. Again, $\alpha = 70^\circ$ and the Gaussian intensity profile, this time centered at $r_{\text{ovc}} = 0.85$, were assumed. In spite of the similar (ie. caustic) nature of the profiles' peaks, the position angle curves and polarization degree predicted by the OG model are completely different than those observed for the Crab. Apparently, this demonstrates the sensitivity of the modelled results to the parameter r_{ovc} . The difficulty of the OG model in reproducing the Crab's data persists for other model parameters. We find that the OG model is not able to reproduce the Crab optical data even qualitatively.

5 Comparison with the outer gap results of RY95

The polarization characteristics shown in Fig. 5 differ significantly from those presented by RY95 in their fig. 5. We argue that our results are superior to those of RY95 because their calculation method was flawed at least in two aspects. First, to take into account contributions of emission from different regions of the magnetosphere at the same rotational phase, they just “averaged the position angles” (see Section 3 in RY95) instead of appropriate handling of the Stokes parameters. Second, they neglected to include the acceleration of an electron due to the corotation of the magnetosphere. The latter effect considerably affects the position angle already at $r \sim 0.1R_{\text{lc}}$, not to mention the vicinity of the light cylinder (cf. fig. 3 in Hibschan & Arons 2001).

Our attempts to reproduce RY95' results for the Crab pulsar (fig. 5 in RY95) fail already at the level of the lightcurve. Fig. 6 presents the radiation pattern on the $(\phi, \zeta_{\text{obs}})$ plane, the lightcurve, the position angle, and the degree of polarization (top to bottom) for the same parameters as in RY95 (ie. $\alpha = 80^\circ$, $\zeta_{\text{obs}} = 62^\circ$). We obtain a different lightcurve even though we exactly followed their prescription for emissivity along magnetic field lines ($F \propto 2s - s^2$, with a gaussian decline above $s = 1$ with $\sigma = 0.5$, see RY95 for details) as well as the same formula for footprints of the gamma-ray bright magnetic field lines ($w = 0.02(70^\circ/\alpha)(r_c/r_{c,\text{min}})$, where $w \approx 1 - r_{\text{ovc}}$, for definitions see RY95). The location of these footprints on the polar cap is shown in Fig. 7 for selected magnetic field lines.

Although we sampled a very large variety of model parameters (including different prescriptions for the emissivity and for the open volume coordinate w), we were not able to obtain the lightcurve and the position angle swing similar to the one in fig. 5 of RY95 for the same α and ζ_{obs} . All evidence we have gathered, and especially the comparison of our radiation pattern with the one obtained by RY95 (R. W. Romani, private communication) suggest that their result was obtained for a “very specialized” selection of the gamma-ray-bright magnetic field lines which differs from the formula given in their paper.

6 Conclusions

None of the models was able to exactly reproduce the optical polarization data on the Crab pulsar. The general features, however, (ie. fast changes of position angle and minima in polarization degree associated with two peaks) find qualitative explanation within the two-pole caustic model.

7 Discussion

Our calculation method was purely geometrical and neglected any details of physics of radiation mechanism(s). The only “high-energy” aspect of this calculation was the radially extended emission region (at radio wavelengths the radial extent is usually assumed to be small). Extension of this work to include microscopic physics would be of great value (cf. Epstein 1973; Chen et al. 1996).

Muslimov & Harding (2004) have recently extended the slot gap acceleration to very high altitudes, which makes the geometry of the slot gap model similar to the TPC model. The accelerating electric field which they propose may be used to model the physics of emission and to improve the polarization calculation for the TPC/slot gap model.

References:

- Chen, K., Chang, H.-K., & Ho, C. 1996, *ApJ*, 471, 967
Cheng, K. S., Ruderman, M. A., & Zhang, L. 2000, *ApJ*, 537, 964
Dyks, J., & Rudak, B., 2003, *ApJ*, 598, 1201
Dyks, J., Harding, A.K., & Rudak, B. 2004, *ApJ*, in press (astro-ph/0401255)
Epstein, R. I., 1973, *ApJ*, 183, 593
Graham-Smith, F., Dolan, J. F., Boyd, P. T., Biggs, J. D., Lyne, A. G., et al. 1996, *MNRAS*, 282, 1354
Hibschman, J. A., & Arons, J. 2001, *ApJ*, 546, 382
Jones, D. H. P., Smith, F. G., & Wallace, P. T. 1981, *MNRAS*, 196, 943
Kanbach, G., Kellner, S., Schrey, F., Steinle, H., Straubmeier, C., et al. 2003, in *Proc. of the SPIE Meeting on Astronomical Telescopes and Instrumentation "Power Telescopes and Instrumentation into the New Millenium"*, eds. Iye, M., & Moorwood, A. F., 4841, 82
Kellner, S., 2002, *Diplomarbeit*, Technische Universität München
Kern, B., Martin, C., Mazin, B., & Halpern, J.P. 2003, *ApJ*, 597, 1049
Muslimov, A.G., & Harding, A.K. 2004, *ApJ*, in press
Romani, R. W. & Yadigaroglu, I.-A., 1995, *ApJ*, 438, 314 (RY95)
Romani, R. W., Miller, A. J., Cabrera, B., Nam, S. W., & Martinis, J. M. 2001, *ApJ*, 563, 221
Smith, F. G., Jones, D. H. P., Dick, J. S. B., & Pike, C. D. 1988, *MNRAS*, 233, 305

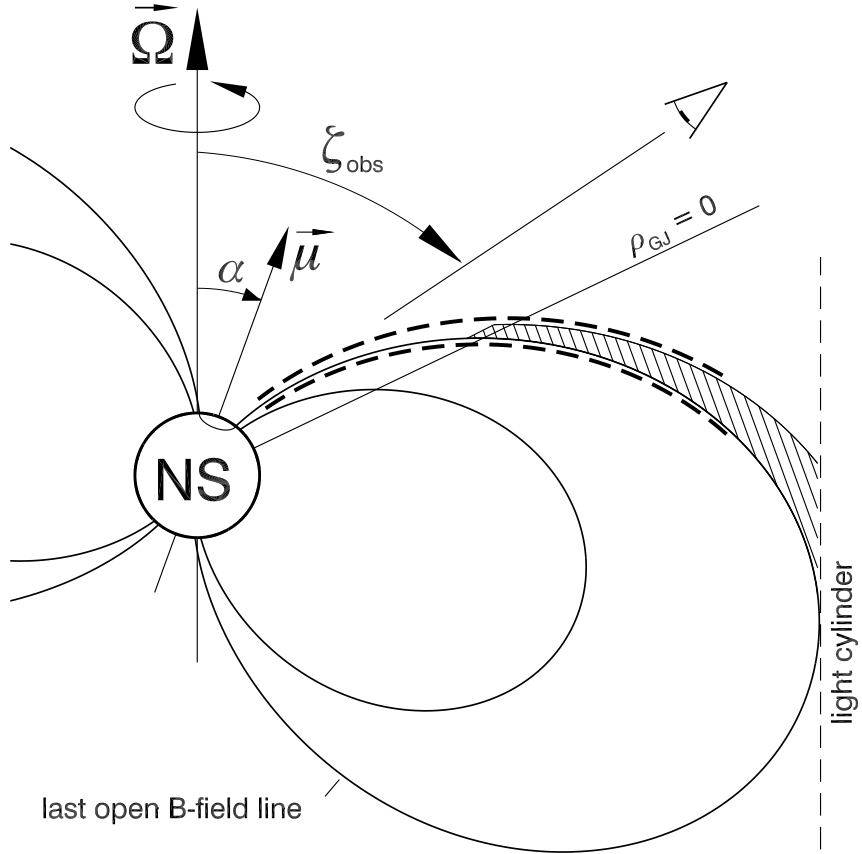


Figure 1: Illustration of the two-pole caustic model. The radiating region (within the dashed lines) is confined to the surface of the last open field lines, and it extends from the polar cap to the light cylinder. For comparison, the conventional outer gap region is shown (shaded area), extending from the surface of the null space-charge ($\rho_{\text{GJ}} = 0$, where $\rho_{\text{GJ}} \approx -\vec{\Omega} \cdot \vec{B}(2\pi c)^{-1}$ is the Goldreich-Julian charge density) to the light cylinder.

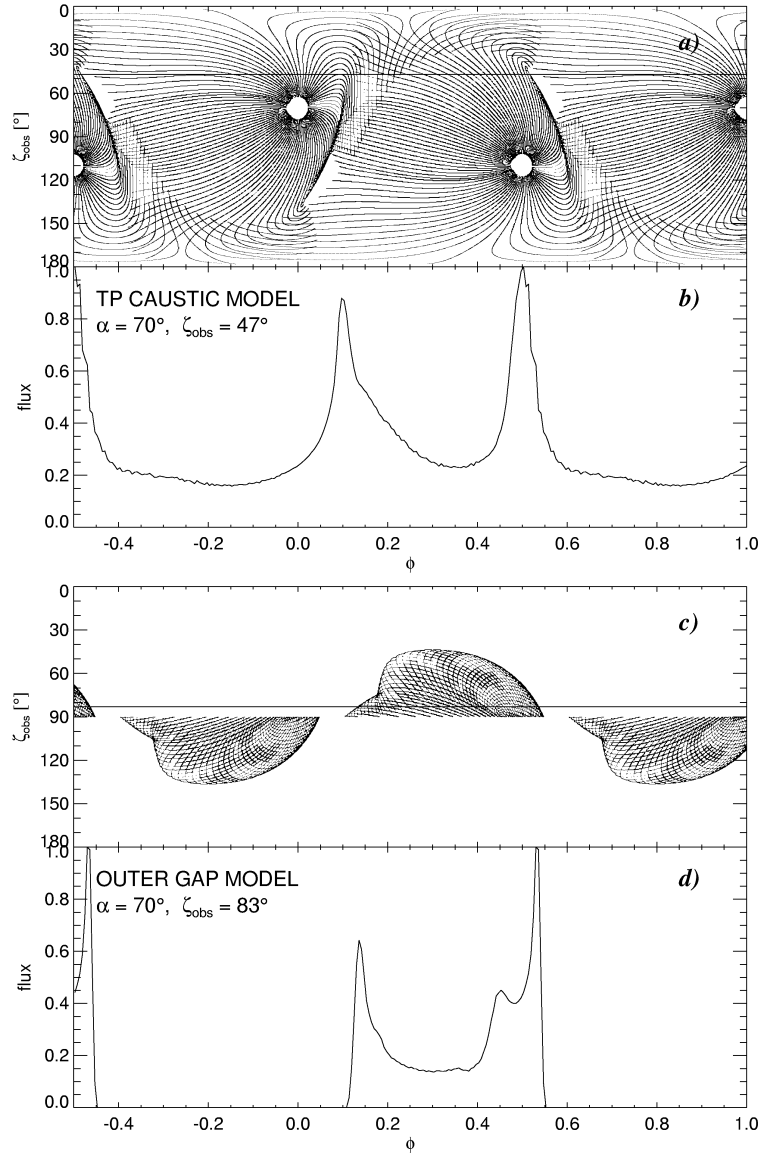


Figure 2: **a)** A pattern of pulsar high-energy emission on the $(\phi, \zeta_{\text{obs}})$ plane calculated with the two-pole caustic model for $\alpha = 70^\circ$, $r_{\text{ovc}} = 1$ (last open B -field lines), $r_{\text{max}} = R_{\text{lc}}$, $\rho_{\text{max}} = 0.8R_{\text{lc}}$ and $P = 0.033$ s. ϕ is the rotational phase, and ζ_{obs} is the viewing angle measured from the rotation axis. **b)** A high-energy lightcurve predicted by the TPC model for an observer located at $\zeta_{\text{obs}} = 47^\circ$, ie. a horizontal crosssection of the pattern from panel **a)** at ζ_{obs} marked with the horizontal line. The transverse gaussian emissivity profile with $\sigma = 0.025$, centered at $r_{\text{ovc}} = 1$ was assumed. **c)** and **d)** – the same as **a)** and **b)** respectively, but for the outer gap model with $\zeta_{\text{obs}} = 83^\circ$, $r_{\text{ovc}} = 0.85$, $r_{\text{max}} = 1.7R_{\text{lc}}$ and $\rho_{\text{max}} = 0.999R_{\text{lc}}$. Note prominent differences between the models.

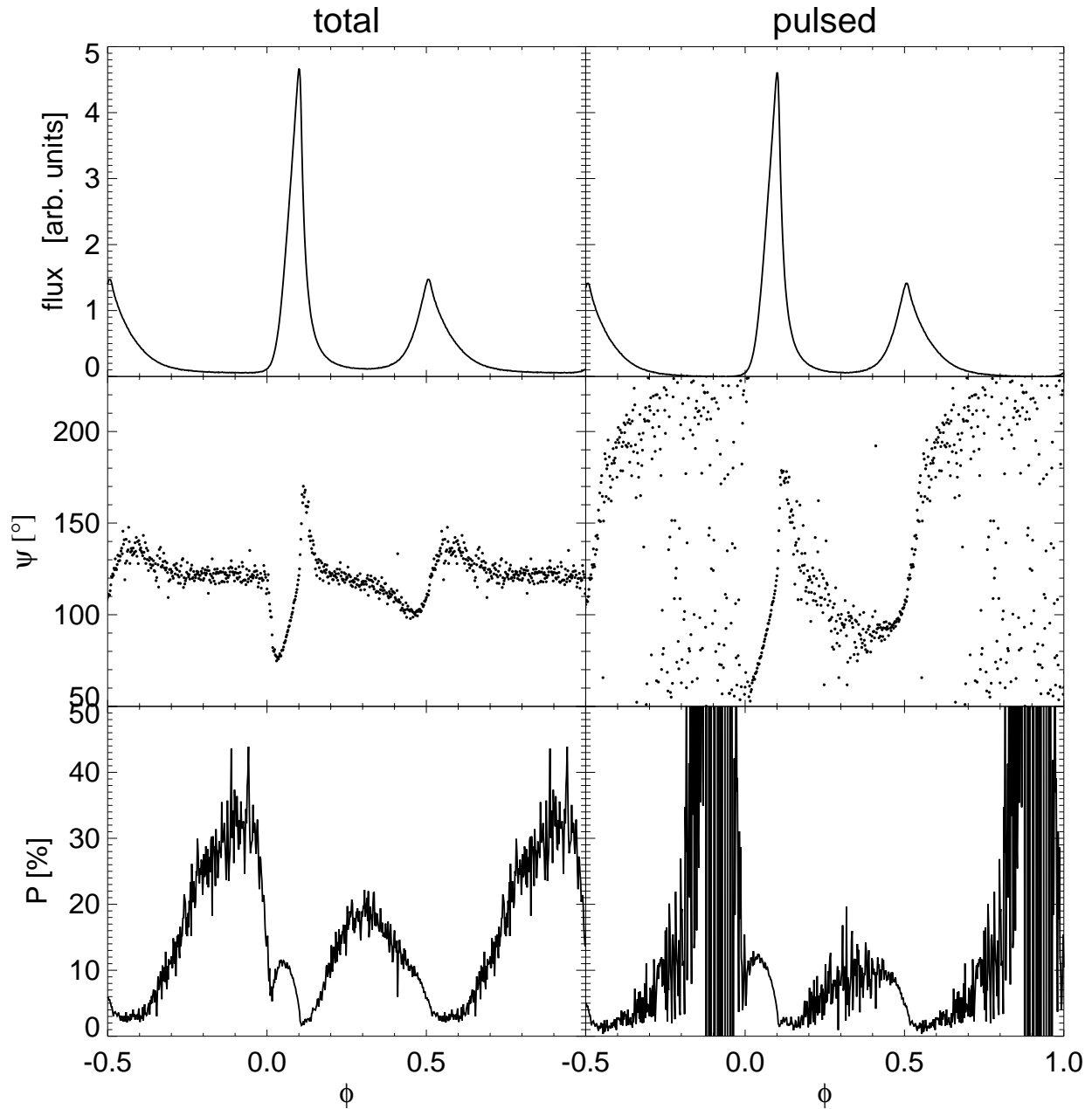


Figure 3: Preliminary optical data on the Crab pulsar obtained with the OPTIMA instrument (Kanbach et al. 2003; this workshop). **Left column:** a lightcurve (top panel), a position angle ψ (dots, middle panel), and a degree of polarization P [%] (bottom panel). The constant value of position angle within phase ranges 0.2–0.3 and 0.7–1.0 suggests that the received radiation consists of two components, one of which has constant properties. **Right column:** same as in the left column but with the contribution of the constant component subtracted from the data. Following Kellner (2002), for the constant component we assumed intensity equal to 1.24 % of the maximum intensity of the total signal, $\psi = 123^\circ$, and $P = 33$ %. One and a half period is shown. The maximum of the leading peak was aligned with the phase $\phi = 0.1$. The data were kindly provided by G. Kanbach.

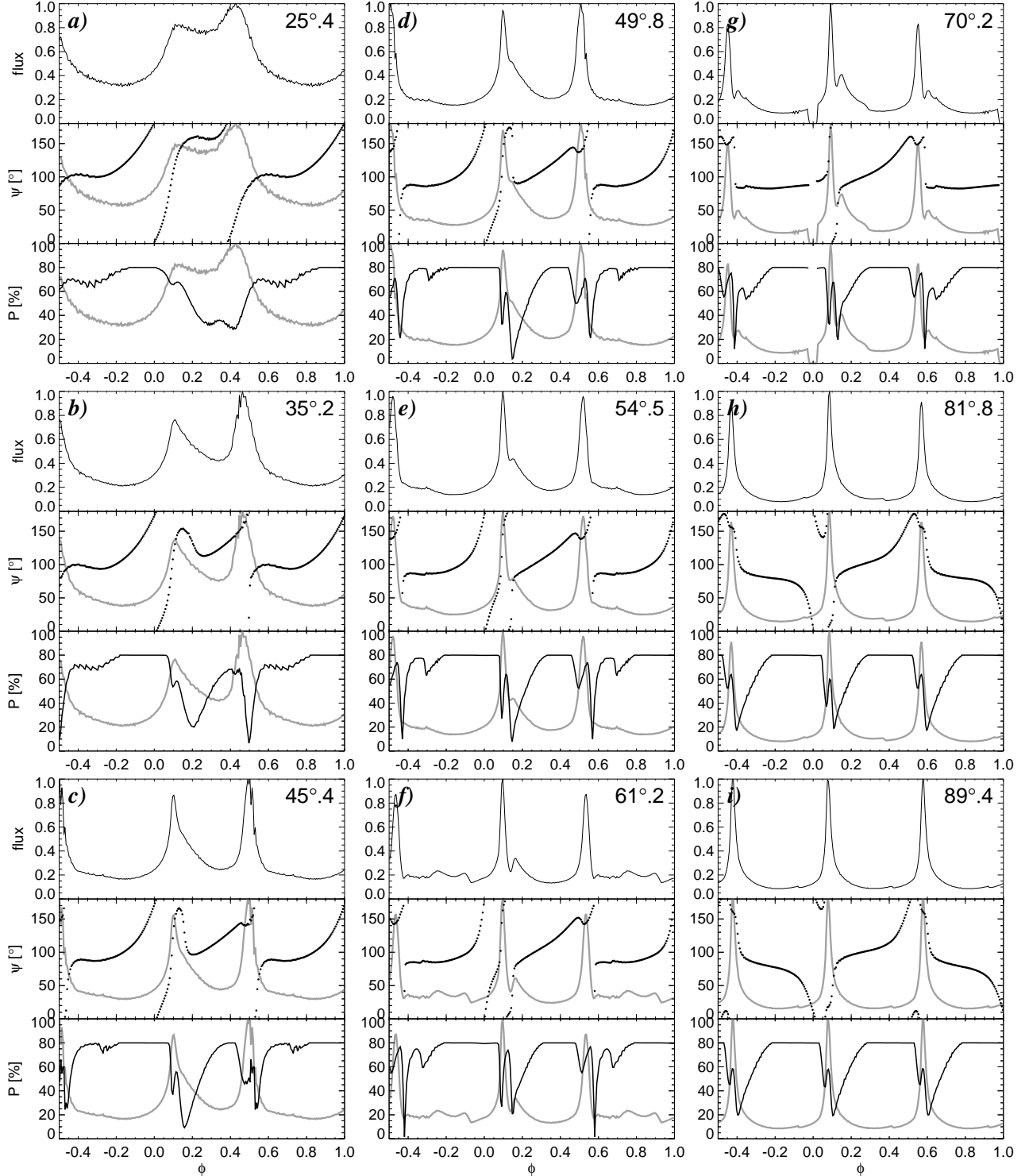


Figure 4: Radiation characteristics predicted by the **two-pole caustic** model for a pulsar with dipole inclination $\alpha = 70^\circ$. Nine three-panel frames correspond to nine different viewing angles ζ_{obs} (marked in the top right corners). Each frame presents the lightcurve (top panel), the position angle curve (dots, middle panel), and the degree of linear polarization (thick solid line, bottom panel). For reference, the lightcurve is overplotted in the middle and in the bottom panels as a thick grey line. Note the dominance of two widely separated peaks in lightcurves for most viewing angles, as well as the fast swings of the position angle and minima in polarization degree at/close to the peaks. The results are for photon emission constrained to $\rho \leq 0.8R_{\text{lc}}$ and $r \leq R_{\text{lc}}$.

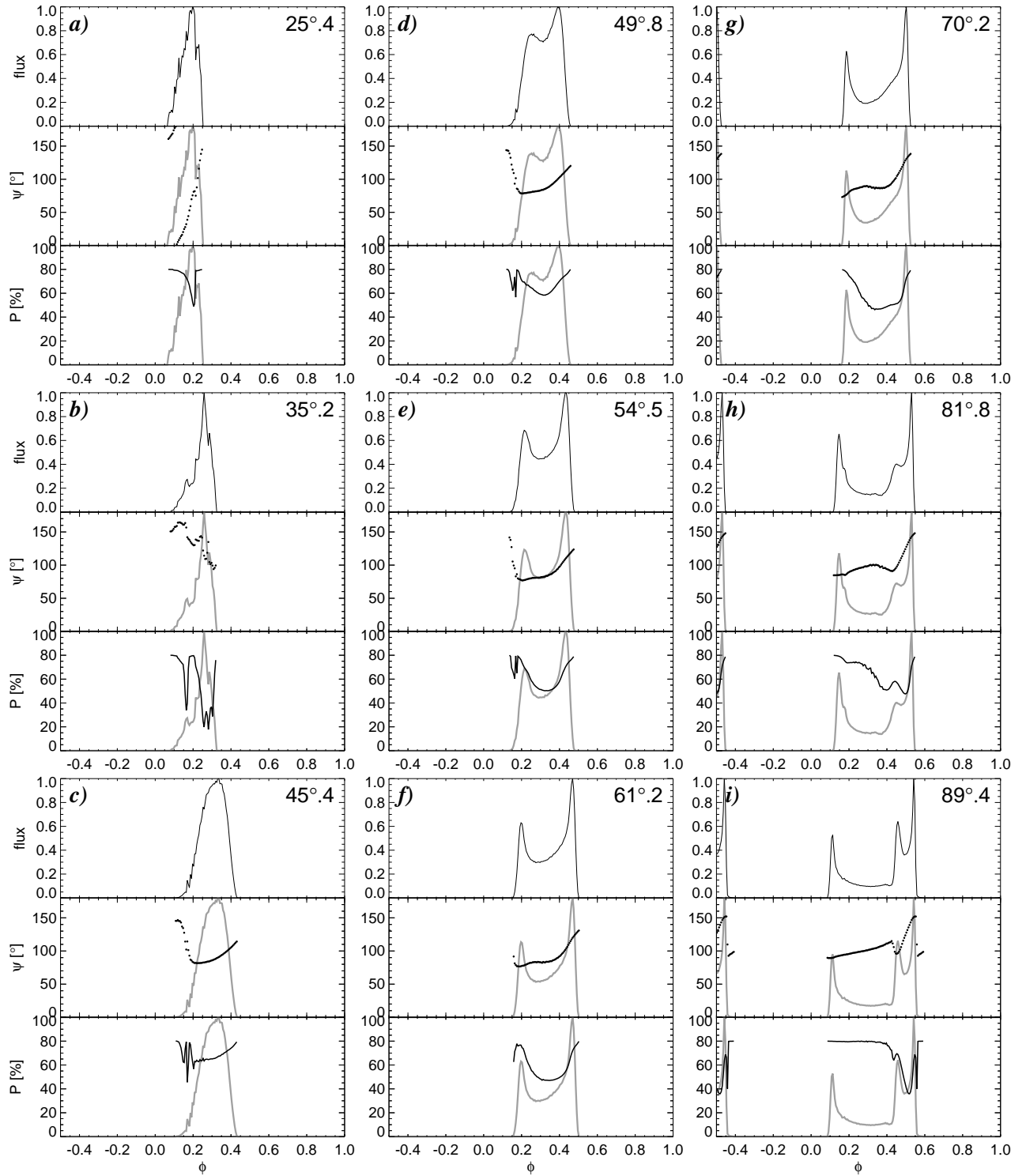


Figure 5: Radiation characteristics predicted by the **outer gap** model for a pulsar with dipole inclination $\alpha = 70^\circ$. The layout is the same as in Fig. 4. Emission region was constrained to $\rho \leq 0.999R_{\text{lc}}$ and $r \leq 1.7R_{\text{lc}}$.

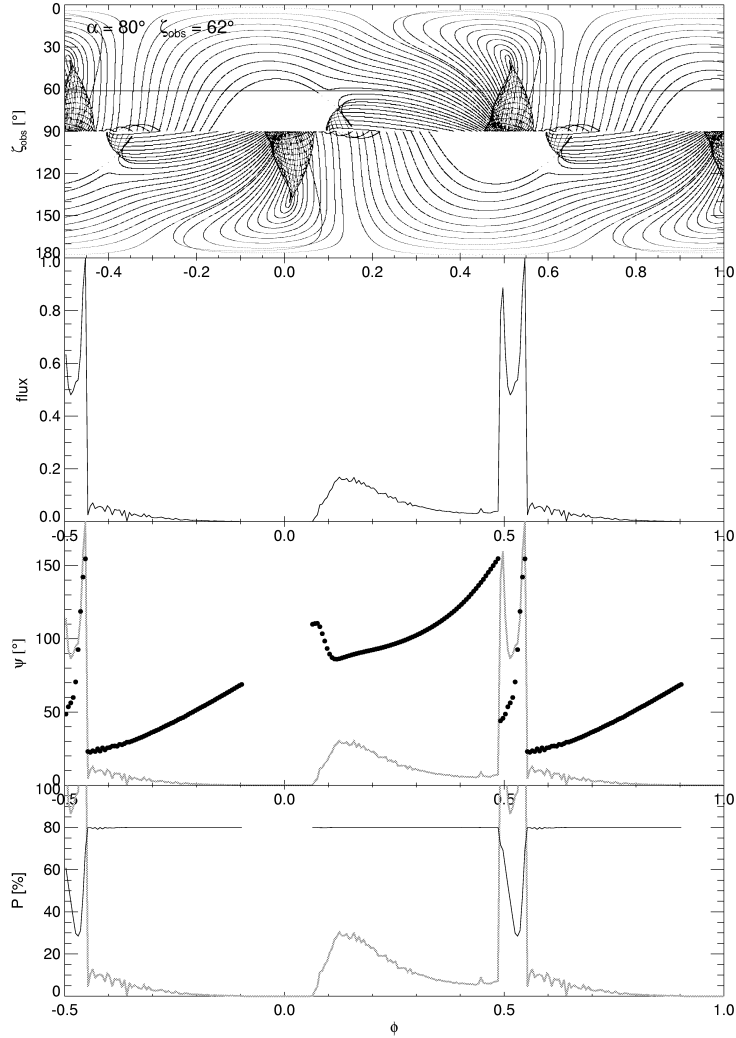


Figure 6: Top to bottom: the radiation pattern, the lightcurve, the position angle curve, and the degree of polarization predicted by the **outer gap** model for the same parameters as in fig. 5 of RY95 ($\alpha = 80^\circ$, $\zeta_{\text{obs}} = 62^\circ$). The emissivity along magnetic field lines as well as the choice of these gamma-ray-bright lines was assumed after RY95. Footprints of some of these lines on the polar cap are shown in the next figure.

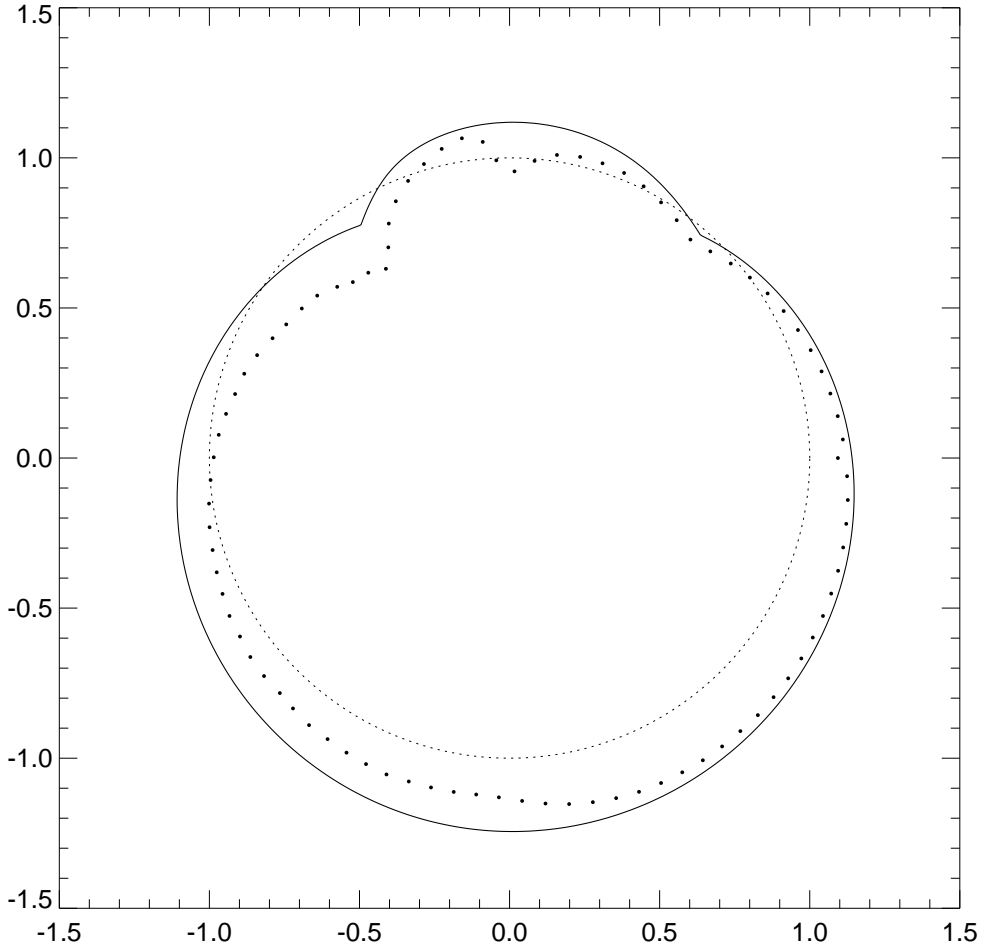


Figure 7: Footprints of the gamma-ray-bright magnetic field lines on the polar cap surface (sparse dots), calculated for $\alpha = 80^\circ$ according to the formula $w = 0.02(70^\circ/\alpha)(r_c/r_{c,\min})$ from RY95. The thick solid line is the rim of the polar cap, and the dotted line is a circle of the standard polar cap radius $r_{\text{pc}} = (R_{\text{NS}}^3/R_{\text{lc}})^{1/2}$. To reproduce the results of RY95, the footprints on the “equatorward” side of the polar cap (on the right-hand side in the figure) would have to lie farther apart from the rim of the polar cap.